An Op-Amp-Based PID Control of DC-DC Buck Converter for Automotive Applications

ANAS BOUTAGHLALINE, KARIM EL KHADIRI, AHMED TAHIRI
Laboratory of Computer Science and Interdisciplinary Physics (L.I.P.I), Normal Superior School,
Sidi Mohamed Ben Abdellah University,
B.P 5206 Bensouda, Fez,
MOROCCO

Abstract: - The present paper introduces the design and simulation of an op-amp-based PID-controlled DC-DC buck converter to regulate a DC voltage of 12 V to 5 V and support load currents ranging from 1 A to 5 A for automotive applications using LTspice software. The converter operates at a switching frequency of 550 kHz, delivering a regulated output voltage of 5 V for load currents ranging from 1 A to 5 A, with a maximum output voltage ripple of 47.56 mV. The proposed buck converter settles to its regulated value within 943.4 µs at a load current of 1 A, with a peak efficiency of 92.83%. The simulation results of the proposed buck converter response to load current fluctuations show that the buck converter settles to its regulated value in 83.36 µs during a load current change from 1 A to 5 A with an undershoot of 92.62 mV. Conversely, during a load change from 5 A to 1 A, the proposed buck converter recovers from an overshoot of 52.04 mV within 46.32 µs.

Key-Words: - Power Management Systems; Switching Converters; DC-DC Buck Converter; PID Controller; Transient Performance; Automotive.

Received: March 28, 2023. Revised: December 11, 2023. Accepted: December 26, 2023. Published: December 31, 2023.

1 Introduction

Energy efficiency is becoming more and more important, in today's automobile applications making efficient power management systems crucial to meet this demand, [1], [2]. One essential component of these power management systems is the DC-DC converter. The DC-DC converters are commonly used in electronic devices like portable electronics, wearable gadgets, Internet of Things (IoT) devices, as well as automotive applications like advanced driver assistance systems (ADAS) hybrid vehicles, and electric vehicles, [3], [4], [5], [6], [7], [8], [9], [10]. There are two types of DC-DC converters: switching and linear. Linear converters are simple to implement but they have low efficiency, especially when V_i is much bigger than V_o, with high heat dissipation, which makes them unsuitable for high-power applications. On the other hand, switching converters offer more efficiency and can handle higher power levels, [11], [12], [13]. A buck converter is a switching converter, and found wide use in automotive applications to reduce DC voltage from a higher level while minimizing power loss, [14], [15], [16], [17]. A feedback control system ensures efficient regulation of the output voltage, using analog or digital implementations, [18], [19], [20], [21]. Control systems with stronger computational capabilities are gaining increasing interest recently. Among these control systems, predictive control techniques have shown good results when applied to power electronics systems. However, one major limitation they face apart, from the complexity is the need to know the mathematical model of the controlled system. Therefore, the use of the predictive control techniques is not suitable for the fast-switching converters, [22], [23], [24], [25], [26], [27]. Also, in recent years have become familiar with the use of artificial intelligence techniques employed in DC-DC converter control, particularly deep learning as well as artificial neural networks, which according to research, possess good potential for effective power converters output voltage regulation, [28], [29], [30], [31]. One of the most popular control strategies for DC-DC converters over the last few years is the proportional-integral-derivative (PID) control strategy. PID control systems reduce steady-state error as well as settling time and overshoot, [32], [33]. PID control uses three components: proportional, integral, and derivative. The proportional component provides a proportionate response to the deviation between the actual and desired output voltage. The integral part gives a proportional response to the error accumulated over time, while the derivative component provides a

proportional response to the rate of change of the error.

The present study aims to design and simulate a DC-DC buck converter with a voltage-mode PID controller for automotive applications, using LTspice, which is an open-source software variant of the Simulation Program with Integrated Circuit Emphasis (Spice). In this research, it is assumed that the proposed converter will provide higher efficiency, stability, and output accuracy than the conventional converters, due to the accurate and fast control over the output voltage of the converter, using an op-amp based PID controller, resulting in a more reliable and efficient power management system.

The remainder of the present paper is structured as follows: Section 2 explains the control strategy and design of the proposed converter. Section 3 presents, compares, and discusses the simulation results. Section 4 serves as the conclusion section of the paper.

2 Methods

The proposed architecture of the buck converter, including the voltage-mode PID controller, is presented in Figure 1. The buck converter is the power stage and consists of four main components: the inductor L, the output capacitor Co, the diode D, and the power switch Q. The proposed converter operates in two stages: the on-time phase and the off-time phase.

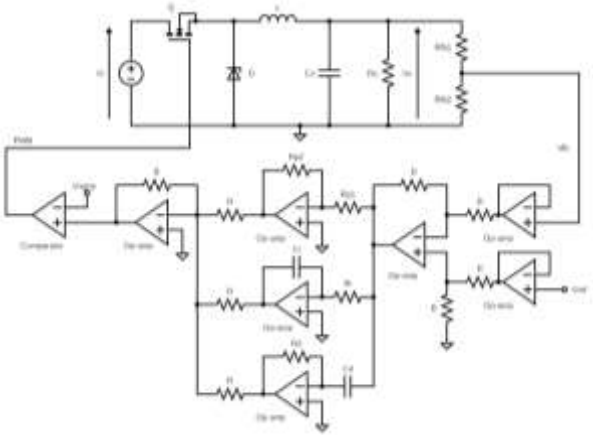

Fig. 1: The proposed DC-DC buck converter with PID control

The buck converter output voltage V_o is expressed as equation (1), where d represents the duty cycle of the switch Q, and V_i is the input voltage. The inductor value L and the output capacitor value C_o can be calculated using equations (2) and (3), respectively, where ΔI_{ind} is the inductor ripple current, f is the switching frequency, and ΔV_o is the output voltage ripple. The op-amp-based controller provides higher accuracy and flexibility in tuning the controller parameters for optimal performance. The feedback signal from the output voltage is fed to the op-amp-based PID controller through a voltage divider based on R_{fb1} and R_{fb2} resistors, as expressed in equation (4). Therefore, the generated feedback voltage is compared with a reference voltage V_{ref} through a subtractor circuit to calculate the error for a reverse-acting controller. As the feedback voltage increases, the error signal decreases. The controller uses a parallel combination of the proportional, integral, and derivative terms to adjust the duty cycle according to the error voltage. The PWM signal with the appropriate duty cycle is then generated by summing the individual terms and comparing the sum result to a ramp voltage signal V_{ramp}.

$$V_o = d \times V_i \tag{1}$$

$$L = (V_i - V_o) \times \frac{d}{f * \Delta I_{ind}} \tag{2}$$

$$C_o = \frac{\Delta I_{ind}}{8 \times f \times \Delta V_o} \tag{3}$$

$$V_o = (1 + \frac{R_{fb2}}{R_{fb1}}) \times V_{ref} \tag{4}$$

The proposed DC-DC buck converter controlled by voltage-mode PID design has the following specifications: an input voltage of 12 V, an output voltage of 5 V, a load current range of 1 A to 5 A, and a switching frequency of 550 kHz. Table 1 summarizes the calculated values of the buck converter components besides its specifications.

Table 1. Buck converter specifications and component values

Parameter/Component	Values
Input voltage	12 V
Output voltage	5 V
Switching frequency	550 kHz
Load current	1 A – 5 A
Maximum output voltage ripple	50 mV
Inductor L	30 µH
Output capacitor C_o	7 µF

2.1 DC-DC Buck Converter Modelling

2.1.1 ON-time Phase

During the on-time phase, switch Q is closed, allowing current to flow through the inductor L. This magnetic field around the inductor increases as a result, and the inductor stores energy, while the

diode is reverse-biased, and the output capacitor C_o supplies the load current. Figure 2 illustrates the operation in the switch-on state. Equations (5), (6), (7), and (8) are derived using Kirchhoff's laws. The buck converter output voltage is expressed in (9) and is equal to the output capacitor voltage.

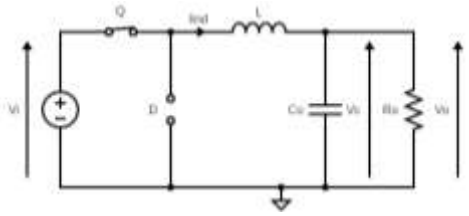

Fig. 2: Buck converter ON-time phase operation

$$V_i - \frac{dI_{ind}}{dt} L - V_c = 0 \quad (5)$$

$$\frac{dI_{ind}}{dt} = \frac{V_i - V_c}{L} \quad (6)$$

$$\frac{V_c}{R_o} + \frac{C_o dV_c}{dt} = I_{ind} \quad (7)$$

$$\frac{dV_c}{dt} = \frac{I_{ind}}{C_o} - \frac{V_c}{R_o C_o} \quad (8)$$

$$V_o = V_c \quad (9)$$

2.1.2 OFF-time Phase

During the off-time phase, the switch Q is open, and the diode is forward-biased. The inductor L discharges the stored energy to the load, and the voltage across the inductor decreases. Figure 3 illustrates the operation in the switch-off state. Equations (10), (11), (12), and (13) are derived using Kirchhoff's laws. The output voltage of the buck converter is expressed in (14) and is equal to the output capacitor voltage.

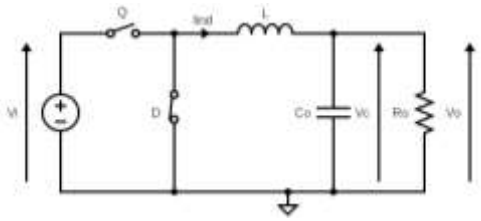

Fig. 3: Buck converter OFF-time phase operation

$$\frac{dI_{ind}}{dt} L + V_c = 0 \quad (10)$$

$$\frac{dI_{ind}}{dt} = \frac{-V_c}{L} \quad (11)$$

$$\frac{V_c}{R_o} + \frac{C_o dV_c}{dt} = I_{ind} \quad (12)$$

$$\frac{dV_c}{dt} = \frac{I_{ind}}{C_o} - \frac{V_c}{R_o C_o} \quad (13)$$

$$V_o = V_c \quad (14)$$

2.1.3 State space Model

A dynamic system is represented linearly in the state space model. It uses a matrix equation to describe a time-invariant linear system. A linear or nonlinear system's performance is frequently modeled using state space models, [34], [35], [36]. The buck converter is a nonlinear system because it is a switching converter. The state space averaging method effectively analyzes nonlinear systems, [37].

The state space model of the ON-time phase is determined based on the equations (6), (8), and (9) and can be expressed as (15) and (16). Furthermore, the state space model of the OFF-time phase is derived using equations (11), (13), and (14) and can be expressed in matrix form as (17) and (18).

$$\begin{bmatrix} \frac{dI_{ind}}{dt} \\ \frac{dV_c}{dt} \end{bmatrix} = \begin{bmatrix} 0 & \frac{1}{C_o} \\ -\frac{1}{L} & -\frac{1}{R_o C_o} \end{bmatrix} \begin{bmatrix} I_{ind} \\ V_c \end{bmatrix} + \begin{bmatrix} \frac{1}{L} \\ 0 \end{bmatrix} V_i \quad (15)$$

$$V_o = [0 \quad 1] \begin{bmatrix} I_{ind} \\ V_c \end{bmatrix} \quad (16)$$

$$\begin{bmatrix} \frac{dI_{ind}}{dt} \\ \frac{dV_c}{dt} \end{bmatrix} = \begin{bmatrix} 0 & \frac{1}{C_o} \\ -\frac{1}{L} & -\frac{1}{R_o C_o} \end{bmatrix} \begin{bmatrix} I_{ind} \\ V_c \end{bmatrix} + \begin{bmatrix} 0 \\ 0 \end{bmatrix} V_i \quad (17)$$

$$V_o = [0 \quad 1] \begin{bmatrix} I_{ind} \\ V_c \end{bmatrix} \quad (18)$$

Assuming that the state variables are $X_2 = I_{ind}$, $X_2 = V_c$, $\dot{X}_1 = \frac{dI_{ind}}{dt}$, $\dot{X}_1 = \frac{dV_c}{dt}$. The output variable is $Y = V_o$, and the input variable is $U = V_i$. From (15), (16), (17), and (18), the state space model of the buck converter during the ON and OFF time phases can be expressed as (19), (20), (21), and (22).

$$\dot{X} = A_1 . X + B_1 . U \quad (19)$$

$$\dot{X} = A_2 . X + B_2 . U \quad (20)$$

$$Y = C_1 . X + D_1 . U \quad (21)$$

$$Y = C_2 . X + D_2 . U \quad (22)$$

Where matrices X, $\dot{X}$, A_1, A_2, B_1, B_2, C_1, C_2, D_1, D_2, U are given by equations (23), (24), (25), (26) and (27):

$$X = \begin{bmatrix} I_{ind} \\ V_c \end{bmatrix} ; \dot{X} = \begin{bmatrix} \frac{dI_{ind}}{dt} \\ \frac{dV_c}{dt} \end{bmatrix} \quad (23)$$

$$A_1 = A_2 = \begin{bmatrix} 0 & \frac{1}{C_o} \\ -\frac{1}{L} & -\frac{1}{R_o C_o} \end{bmatrix} \quad (24)$$

$$B_1 = \begin{bmatrix} \frac{1}{L} \\ 0 \end{bmatrix} ; B_2 = \begin{bmatrix} 0 \\ 0 \end{bmatrix} \quad (25)$$

$$C_1 = C_2 = [0 \quad 1] \quad (26)$$

$$D_1 = D_2 = 0 \quad (27)$$

Then, using the state space averaging method with equations (28), (29), (30), and (31), the matrices A, B, C, and D are calculated. The duty cycle of the ON and OFF time phases is indicated by the terms "d" and "(1-d)", respectively, [37], [38], [39].

$$A = A_1.d + A_2.(1-d) \quad (28)$$

$$B = B_1.d + B_2.(1-d) \quad (29)$$

$$C = C_1.d + C_2.(1-d) \quad (30)$$

$$D = D_1.d + D_2.(1-d) \quad (31)$$

Therefore, matrices A, B, C, and D are expressed in (32), (33), (34), and (35). The buck converter system's complete state space model is represented by equations (36) and (37).

$$A = \begin{bmatrix} 0 & \frac{1}{C_o} \\ -\frac{1}{L} & -\frac{1}{R_o C_o} \end{bmatrix} \quad (32)$$

$$B = d.\begin{bmatrix} \frac{1}{L} \\ 0 \end{bmatrix} \quad (33)$$

$$C = [0 \quad 1] \quad (34)$$

$$D = 0 \quad (35)$$

$$\dot{X} = \begin{bmatrix} 0 & \frac{1}{C_o} \\ -\frac{1}{L} & -\frac{1}{R_o C_o} \end{bmatrix} X + d.\begin{bmatrix} \frac{1}{L} \\ 0 \end{bmatrix} U \quad (36)$$

$$Y = [0 \quad 1]\, X \quad (37)$$

Based on the buck converter state space model given in (36) and (37) and its component values from Table 1, a systematic procedure to examine the buck converter stability. Initially, the characteristic equation was formulated using (38). Subsequently, the system matrix A was substituted with the relevant coefficients, leading to the expression (39). The characteristic equation was then derived by simplifying the determinant, resulting in (40). Numerical substitution of the given values further transformed the equation into (41). Subsequent calculation of the discriminant Δ confirmed its positivity, $\Delta = 1360544215.6462 > 0$, paving the way for applying the quadratic formula. The roots $s_1 = -52985.793599$ and $s_2 = -89871.34925$ were obtained, and their negative values indicated that both poles reside in the left half of the s-plane, as indicated in the root locus plot shown in Figure 4. Consequently, the conclusion was that the system is stable under these conditions.

$$det[sI - A] = 0 \quad (38)$$

$$det\begin{bmatrix} s & -\frac{1}{C_o} \\ \frac{1}{L} & s + \frac{1}{R_o C_o} \end{bmatrix} = 0 \quad (39)$$

$$s^2 + \frac{1}{R_o C_o} s + \frac{1}{L C_o} = 0 \quad (40)$$

$$s^2 + 142857.143\, s + 4761904761.905 = 0 \quad (41)$$

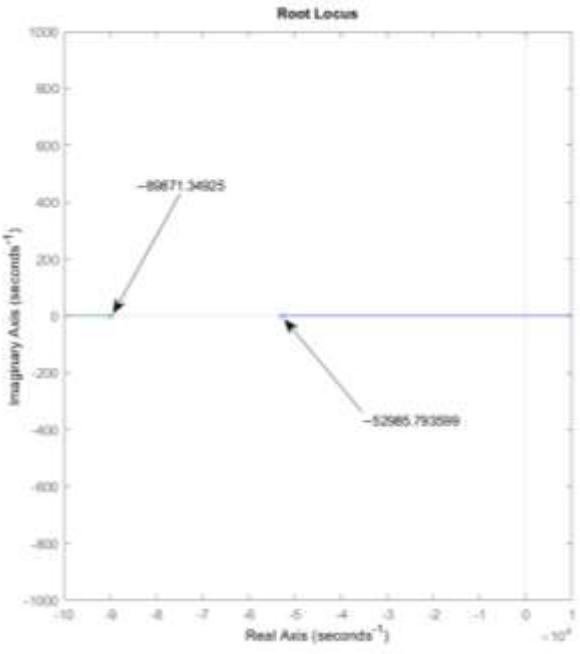

Fig. 4: Root locus plot

2.1.4 Transfer Function

The transfer function can be obtained according to the state space model presented in (36) and (37).

Equations (42) and (43) yield the Laplace transform of (36).

$$s.X = A.X + B.U \quad (42)$$

$$X = (sI - A)^{-1}.B.U \quad (43)$$

Equation (44) expresses the output voltage by substituting (43) with (37). Therefore, (45) can be used to represent the buck converter transfer function.

$$Y = C.(sI - A)^{-1}.B.U + D.U \quad (44)$$

$$\frac{Y}{U} = C.(sI - A)^{-1}.B + D \quad (45)$$

Following the A, B, C, and D matrix values being substituted into (45), equations (46) and (47) describe the buck converter transfer function. It incorporates the input voltage V_i, the load resistance R_o, and the inductor's inductance L, where $V_o(s)$ is the buck converter output voltage and d(s) represent the duty cycle ratio.

$$\frac{V_o(s)}{V_i(s)} = \frac{d}{LC_oS^2+\frac{L}{R_o}s+1} \quad (46)$$

$$G_p(s) = \frac{V_o(s)}{d(s)} = \frac{V_i}{LC_oS^2+\frac{L}{R_o}s+1} \quad (47)$$

2.2 Op-Amp Based PID Controller Design

To design the op-amp-based PID controller for the buck converter, the system's transfer function in closed-loop is needed to define the controller parameters for stable and fast response, as well as minimal steady-state error. Figure 5 shows the block diagram of the system. Through combining, as given in equation (48), the transfer functions of the PID controller $G_c(s)$ with the buck converter $G_p(s)$, the transfer function of the system in closed-loop $G_{cl}(s)$ can be written as equations (49) and (50), where $V_{ref}(s)$ denotes the reference voltage. By making the coefficients of (51) parts equal, K_p, K_i, and K_d can be expressed as equations (52), (53), and (54), respectively.

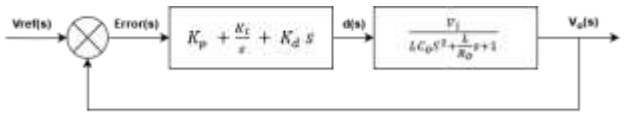

Fig. 5: System block diagram

$$G_c(s) = \frac{d(s)}{Error(s)} = K_p + \frac{K_i}{s} + K_d s \quad (48)$$

$$Gcl(s) = \frac{V_o(s)}{Vref(s)} = \frac{G_p(s)G_c(s)}{1+G_p(s)G_c(s)} \quad (49)$$

$$Gcl(s) = \frac{(K_d s^2+K_p s+K_i)\times V_i}{\left(LC_o s^2+\frac{L}{R_o}s+1\right)s+(K_d s^2+K_p s+K_i)\times V_i} \quad (50)$$

$$LC_o s^2 + \frac{L}{R_o} s + 1 = K_d s^2 + K_p s + K_i \quad (51)$$

$$K_p = \left|-\frac{R_{p2}}{R_{p1}}\right| = \frac{L}{R_o} \quad (52)$$

$$K_i = \left|-\frac{1}{sR_iC_i}\right| = 1 \quad (53)$$

$$K_d = |-sR_dC_d| = LC_o \quad (54)$$

3 Discussion

The transient analysis results of the proposed buck converter were obtained using LTspice software with an input voltage of 12 V, and a load current ranging from 1A to 5 A. Figure 6 illustrates the transient response of the output voltage to a load current of 1 A. The output voltage converges to its steady state value of 4.99722 V within 943.4 µs, with a ripple voltage of 5.59 mV. The overshoot in the output voltage during the start-up phase is 5.56 V. The efficiency of the system is 92.78%. Figure 7 illustrates the transient response of the output voltage to a load current of 2.5 A. The output voltage stabilizes at its regulated value of 4.99973 V within 614.17 µs, with a ripple voltage of 33.37 mV, and an overshoot in the output voltage during the start-up phase of 5.52 V. The efficiency of the system is 92.83%. Figure 8 demonstrates the transient response of the output voltage to a load current of 5 A. The output voltage settles to its steady state value of 4.99906 V within 521.68 µs, with a ripple voltage of 47.56 mV, and an overshoot at output voltage during the start-up phase of 5.45 V. The efficiency of the system is 90.86%.

In comparison to the finding of [40], where the transient output voltage reaches a steady state at 10 ms for a load of 1 A, the output voltage of the presented converter settles to the target value faster.

In particular, the transient output voltage response to a change in load current from 1 A to 5 A and back from 5 A to 1 A, depicted in Figure 9, demonstrates the system's fast response. The system settles to the regulated value with an undershoot voltage of 92.62 mV and an overshoot voltage of 52.04 mV, while the recovery time is 83.36 µs and 46.32 µs, respectively.

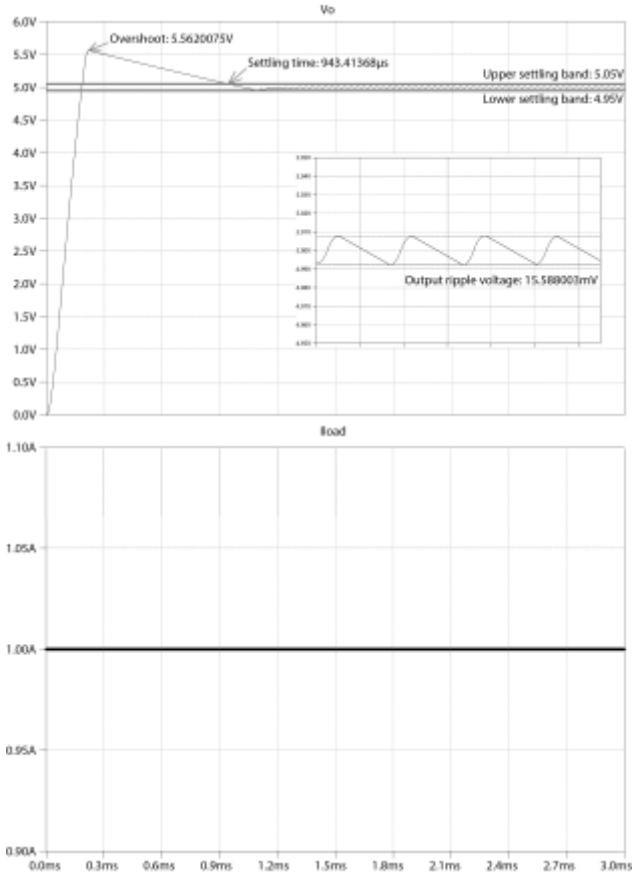

Fig. 6: 1 A load current transient response

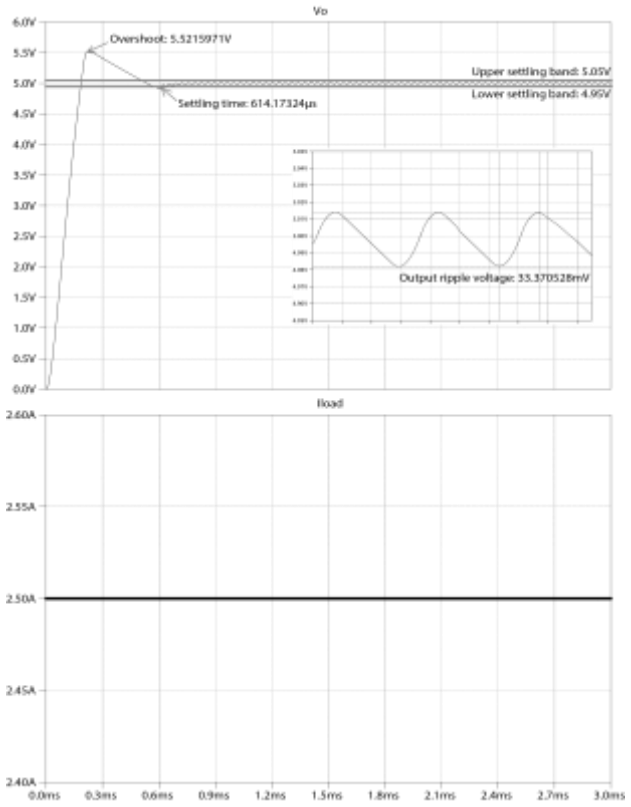

Fig. 7: 2.5 A load current transient response

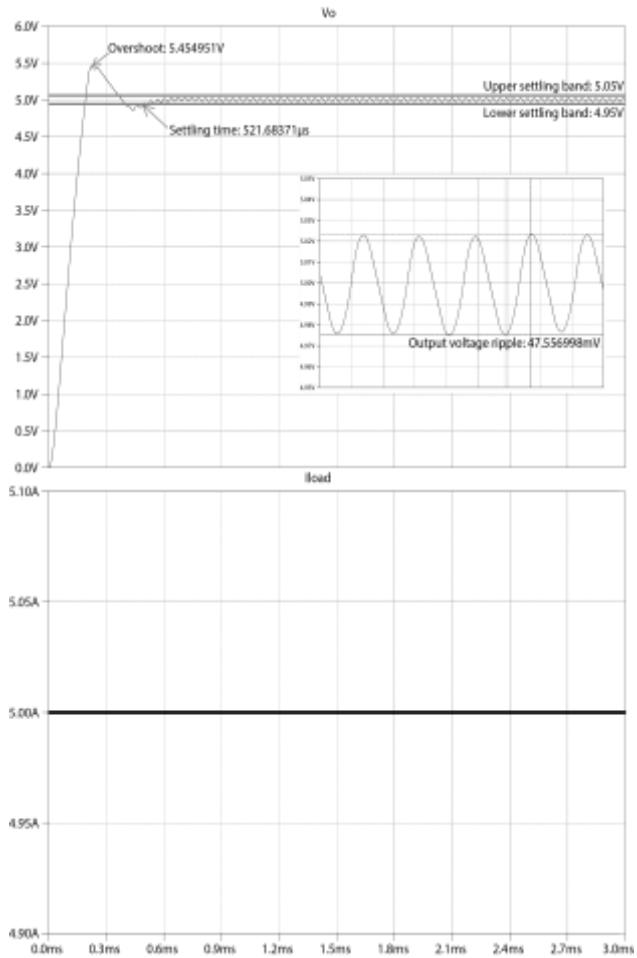

Fig. 8: 5 A load current transient response

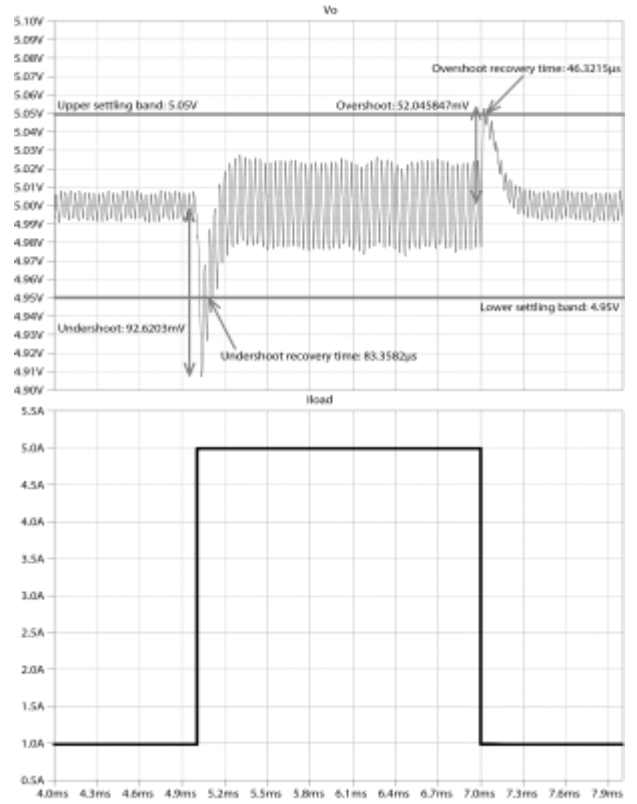

Fig. 9: Load change transient response

A comparison with prior studies, based on the figure of merit (FOM) formula provided in (55) is summarized in Table 2, and reveals that the proposed buck converter with PID control in voltage mode can produce the targeted output voltage across the range of load currents while responding quickly to variations in the load current.

$$FOM = \frac{Peak\ Efficiency\ (\%) \times Step\ Load\ Change\ (mA)}{Max\ Tran.Voltage(mV) \times Max\ Tran.\ Response\ (\mu s)} \times 10^{-2} \quad (55)$$

Table 2. The performance comparison of the presented buck converter with previous works

References	[41]	[42]	This work
Input voltage	12V	12 V	12V
Output voltage	5V	5V	5V
Load current	0.4A–2A	1A-2A	1A–5A
Step load change	1.6A	1A	4A
Undershoot/ Overshoot recovery time	NA/ 500µs	NA/ 200µs	83.36µs/ 46.32µs
Undershoot/ Overshoot	NA/ 300mV	NA/ 380mV	92.62mV/ 52.04mV
Peak efficiency	99.29%	99.61%	92.83%
FOM	0.0106	0.013	0.48

4 Conclusion

This paper successfully presents a voltage mode operational amplifier-based PID controller for a buck converter. The designed buck converter demonstrated exemplary performance in response to changes in load current from 1 A to 5 A. Its output voltage settles to the targeted value within 943.4 µs. The proposed converter recovers during load change with an undershoot voltage of 92.62 mV, an overshoot voltage of 52.04 mV, and a recovery time of 83.36 µs and 46.32 µs, respectively. The peak efficiency is 92.83%, and the maximum output voltage ripple is 47.56 mV. These results demonstrate the effectiveness of the PID control method in regulating the output voltage. To enhance the transient performances and power efficiency of the buck converter, it may be possible to conduct further research on digital control strategies through artificial intelligence methods, especially neural networks, and deep learning control methodologies, in the future. Another recommendation for future work is designing the converter at the layout level in the 180nm CMOS process to determine the total chip area.

Acknowledgement:
This work was funded by the PPR2 program of the National Center for Scientific and Technical Research (CNRST Morocco).

References:

[1] P. K. Maroti, S. Padmanaban, M. S. Bhaskar, V. K. Ramachandaramurthy, and F. Blaabjerg, "The state-of-the-art of power electronics converters configurations in electric vehicle technologies," *Power Electron. Devices Components*, vol. 1, p. 100001, Mar. 2022, doi: 10.1016/J.PEDC.2021.100001.

[2] A. Boutaghlaline, K. El Khadiri, and A. Tahiri, "An on-chip soft-start pseudo-current hysteresis-controlled buck converter for automotive applications," *Int. J. Electr. Comput. Eng.*, vol. 14, no. 2, pp. 1459–1472, Apr. 2024, doi: 10.11591/IJECE.V14I2.PP1459-1472.

[3] C. González-Castaño, C. Restrepo, F. Flores-Bahamonde, and J. Rodriguez, "A Composite DC–DC Converter Based on the Versatile Buck–Boost Topology for Electric Vehicle Applications," *Sensors 2022, Vol. 22, Page 5409*, vol. 22, no. 14, p. 5409, Jul. 2022, doi: 10.3390/S22145409.

[4] K. V. Ramana, S. Majhi, and A. K. Gogoi, "Modeling and Estimation of DC-DC Buck Converter Dynamics Using Relay Feedback Output With Performance Evaluation," *IEEE Trans. Circuits Syst. II Express Briefs*, vol. 66, no. 3, pp. 427–431, Mar. 2019, doi: 10.1109/TCSII.2018.2843526.

[5] J. Wang, hihua Li, J. Yang, B. Wu, and Q. Li, "Finite-time disturbance observer based non-singular terminal sliding-mode control for pulse width modulation based DC–DC buck converters with mismatched load disturbances," *IET Power Electron.*, vol. 9, no. 9, pp. 1995–2002, Jul. 2016, doi: 10.1049/IET-PEL.2015.0178.

[6] K. El Khadiri, H. Akhmal, and H. Qjidaa, "Li-ion battery charging with a buck-boost DC-DC converter for a portable device power management," *J. Low Power Electron.*, vol. 13, no. 2, pp. 263–270, Jun. 2017, doi: 10.1166/JOLPE.2017.1479.

[7] J. J. Chen, Y. S. Hwang, H. W. Chiu, M. D. Luo, C. H. Lai, and J. Ku, "A New Low-Noise I-Squared Buck Converter Suitable for Wireless Sensor Networks With Dual-Current-Acceleration Techniques," *IEEE*

Access, vol. 11, pp. 41644–41653, 2023, doi: 10.1109/ACCESS.2023.3269420.

[8] D. H. Jung, K. Kim, S. Joo, and S. O. Jung, "0.293-mm2 Fast Transient Response Hysteretic Quasi-V2 DC-DC Converter with Area-Efficient Time-Domain-Based Controller in 0.35-μm CMOS," *IEEE J. Solid-State Circuits*, vol. 53, no. 6, pp. 1844–1855, Jun. 2018, doi: 10.1109/JSSC.2018.2805884.

[9] D. Serpanos and M. Wolf, "Internet-of-things (IoT) systems: Architectures, algorithms, methodologies," *Internet-of-Things Syst. Archit. Algorithms, Methodol.*, pp. 1–95, Nov. 2017, doi: 10.1007/978-3-319-69715-4/COVER.

[10] H. Nam, Y. Ahn, and J. Roh, "A buck converter with adaptive on-time PFM control and adjustable output voltage," *Analog Integr. Circuits Signal Process.*, vol. 71, no. 2, pp. 327–332, May 2012, doi: 10.1007/S10470-011-9802-7/METRICS.

[11] N. Sedaghati, H. Martinez-Garcia, and J. Cosp-Vilella, "On modeling of linear-assisted DC-DC voltage regulators," *2016 Conf. Des. Circuits Integr. Syst. DCIS 2016 - Proc.*, pp. 109–112, Feb. 2017, doi: 10.1109/DCIS.2016.7845362.

[12] H. Martínez and A. Conesa, "Modeling of linear-assisted DC-DC converters," *Eur. Conf. Circuit Theory Des. 2007, ECCTD 2007*, pp. 611–614, 2007, doi: 10.1109/ECCTD.2007.4529670.

[13] A. Boutaghlaline, K. El Khadiri, and A. Tahiri, "An improved transient performance boost converter using pseudo-current hysteresis control," *Bull. Electr. Eng. Informatics*, vol. 12, no. 6, pp. 3416–3427, Dec. 2023, doi: 10.11591/EEI.V12I6.5835.

[14] H. H. Chou, W. H. Luo, H. L. Chen, and S. F. Wang, "A Novel Buck Converter with Dual Loops Control Mechanism," *Electron. 2022, Vol. 11, Page 1256*, vol. 11, no. 8, p. 1256, Apr. 2022, doi: 10.3390/ELECTRONICS11081256.

[15] C. Hisar, I. Sefa, and N. Altin, "Processor-in-The-Loop Simulation of an Interleaved Buck Converter with MATLAB/Simulink," *Proc. 13th Int. Conf. Electron. Comput. Artif. Intell. ECAI 2021*, Jul. 2021, doi: 10.1109/ECAI52376.2021.9515058.

[16] R. Wani, S. L. Patil, and P. Shinde, "Modeling and Simulation of Average Current-Mode Controlled Bidirectional Multiphase DC-DC Converters used in Hybrid Vehicles," *2021 6th Int. Conf. Converg. Technol. I2CT 2021*, Apr. 2021, doi: 10.1109/I2CT51068.2021.9418219.

[17] J. J. Chen, Y. S. Hwang, S. H. Ho, C. H. Lai, and Y. Ku, "An Improved Low-EMI Fast-Transient-Response Buck Converter Suitable for Wireless Sensor Networks With New Transient Accelerated Techniques," *IEEE Sens. J.*, vol. 22, no. 8, pp. 8234–8244, Apr. 2022, doi: 10.1109/JSEN.2022.3158738.

[18] A. Boutaghlaline, K. El Khadiri, H. Qjidaa, and A. Tahiri, "Design of a Non-inverting Buck-Boost Converter Controlled by Voltage-Mode PWM in TSMC 180 nm CMOS Technology," *Lect. Notes Networks Syst.*, vol. 211 LNNS, pp. 1619–1629, 2021, doi: 10.1007/978-3-030-73882-2_147.

[19] Z. Xiao, J. Ren, Y. Xu, Y. Wang, G. Zhao, C. Lu, and W. Hu, "An automatic slope compensation adjustment technique for peak-current mode DC-DC converters," *AEU - Int. J. Electron. Commun.*, vol. 110, p. 152860, Oct. 2019, doi: 10.1016/J.AEUE.2019.152860.

[20] L. Huang, P. Luo, C. Wang, and X. Zhou, "A High Speed On-Chip Soft-Start Technique With High Start-Up Stability for Current-Mode DC-DC Converter," *IEEE Access*, vol. 7, pp. 27579–27585, 2019, doi: 10.1109/ACCESS.2019.2901529.

[21] Y. S. Hwang, J. J. Chen, J. X. Xu, H. S. Yang, C. H. Lai, and Y. Ku, "An Improved Fast-Transient-Response Low-Transient-Voltage Boost Converter with Pseudo-Current Hysteresis-Controlled Techniques," *IEEE Access*, vol. 9, pp. 127270–127277, 2021, doi: 10.1109/ACCESS.2021.3112065.

[22] M. Lešo, J. Žilková, M. Biroš, and P. Talian, "SURVEY OF CONTROL METHODS FOR DC-DC CONVERTERS," *Acta Electrotech. Inform.*, vol. 18, no. 3, pp. 41–46, Sep. 2018, doi: 10.15546/AEEI-2018-0024.

[23] S. Vazquez, J. I. Leon, L. G. Franquelo, J. Rodriguez, H. A. Young, A. Marquez, and P. Zanchetta, "Model predictive control: A review of its applications in power electronics," *IEEE Ind. Electron. Mag.*, vol. 8, no. 1, pp. 16–31, 2014, doi: 10.1109/MIE.2013.2290138.

[24] H. Maruta, M. Motomura, and F. Kurokawa, "Characteristics study of neural network aided digital control for DC-DC converter," *2014 Int. Power Electron. Conf. IPEC-Hiroshima - ECCE Asia 2014*, pp. 3611–

3615, 2014, doi: 10.1109/IPEC.2014.6870017.

[25] N. Bajoria, P. Sahu, R. K. Nema, and S. Nema, "Overview of different control schemes used for controlling of DC-DC converters," *Int. Conf. Electr. Power Energy Syst. ICEPES 2016*, pp. 75–82, May 2017, doi: 10.1109/ICEPES.2016.7915909.

[26] Q. Guo, I. Bahri, D. Diallo, and E. Berthelot, "Model predictive control and linear control of DC–DC boost converter in low voltage DC microgrid: An experimental comparative study," *Control Eng. Pract.*, vol. 131, p. 105387, Feb. 2023, doi: 10.1016/J.CONENGPRAC.2022.105387.

[27] A. Garces-Ruiz, S. Riffo, C. Gonzalez-Castano, and C. Restrepo, "Model Predictive Control with Stability Guarantee for Second-Order DC/DC Converters," *IEEE Trans. Ind. Electron.*, May 2023, doi: 10.1109/TIE.2023.3283706.

[28] B. K. Bose, "Neural network applications in power electronics and motor drives - An introduction and perspective," *IEEE Trans. Ind. Electron.*, vol. 54, no. 1, pp. 14–33, Feb. 2007, doi: 10.1109/TIE.2006.888683.

[29] W. Dong, S. Li, X. Fu, Z. Li, M. Fairbank, and Y. Gao, "Control of a Buck DC/DC Converter Using Approximate Dynamic Programming and Artificial Neural Networks," *IEEE Trans. Circuits Syst. I Regul. Pap.*, vol. 68, no. 4, pp. 1760–1768, Apr. 2021, doi: 10.1109/TCSI.2021.3053468.

[30] S. Zhang, O. Wallscheid, and M. Porrmann, "Machine Learning for the Control and Monitoring of Electric Machine Drives: Advances and Trends," *IEEE Open J. Ind. Appl.*, vol. 4, pp. 188–214, 2023, doi: 10.1109/OJIA.2023.3284717.

[31] Y. Xiang, H. S. H. Chung, R. Shen, and A. W. lun Lo, "An ANN-Based Output-Error-Driven Incremental Model Predictive Control for Buck Converter Against Parameter Variations," *IEEE J. Emerg. Sel. Top. Power Electron.*, 2023, doi: 10.1109/JESTPE.2023.3253561.

[32] S. K. Ram, N. Kumar, B. K. Verma, A. Abhishek, R. Ranjan, S. Mishra, and S. A. Akbar, "Analysis of Interleaved DC-DC Converter using ANFIS Control for EV Charging Applications," *Proc. 6th Int. Conf. Inven. Comput. Technol. ICICT 2021*, pp. 374–378, Jan. 2021, doi: 10.1109/ICICT50816.2021.9358606.

[33] K. H. Ang, G. Chong, and Y. Li, "PID control system analysis, design, and technology," *IEEE Trans. Control Syst. Technol.*, vol. 13, no. 4, pp. 559–576, Jul. 2005, doi: 10.1109/TCST.2005.847331.

[34] R. H. G. Tan and L. Y. H. Hoo, "DC-DC converter modeling and simulation using state space approach," *2015 IEEE Conf. Energy Conversion, CENCON 2015*, pp. 42–47, 2015, doi: 10.1109/CENCON.2015.7409511.

[35] A. Sarwar, A. Shahid, A. Hudaif, U. Gupta, and M. Wahab, "Generalized state-space model for an n-phase interleaved buck-boost converter," *2017 4th IEEE Uttar Pradesh Sect. Int. Conf. Electr. Comput. Electron. UPCON 2017*, vol. 2018-January, pp. 62–67, Jun. 2017, doi: 10.1109/UPCON.2017.8251023.

[36] U. Javaid and D. Dujic, "Arbitrary order generalized state space average modeling of switching converters," *2015 IEEE Energy Convers. Congr. Expo. ECCE 2015*, pp. 6399–6406, Oct. 2015, doi: 10.1109/ECCE.2015.7310556.

[37] G. Suman, B. V. S. P. Kumar, M. S. Kumar, B. C. Babu, and K. R. Subhashini, "Modeling, analysis and design of synchronous buck converter using state space averaging technique for PV energy system," *Proc. - 2012 Int. Symp. Electron. Syst. Des. ISED 2012*, pp. 281–285, 2012, doi: 10.1109/ISED.2012.27.

[38] P. Azer and A. Emadi, "Generalized state space average model for multi-phase interleaved buck, boost and buck-boost DC-DC converters: Transient, steady-state and switching dynamics," *IEEE Access*, vol. 8, pp. 77735–77745, 2020, doi: 10.1109/ACCESS.2020.2987277.

[39] A. C. Schittler, D. Pappis, C. Rech, A. Campos, and M. A. Dalla Costa, "Generalized state-space model for the interleaved buck converter," *COBEP 2011 - 11th Brazilian Power Electron. Conf.*, pp. 451–457, 2011, doi: 10.1109/COBEP.2011.6085305.

[40] A. S. Samosir, T. Sutikno, and L. Mardiyah, "Simple formula for designing the PID controller of a DC-DC buck converter," *Int. J. Power Electron. Drive Syst.*, vol. 14, no. 1, pp. 327–336, Mar. 2023, doi: 10.11591/IJPEDS.V14.I1.PP327-336.

[41] N. Shinde, S. Sankad, and S. L. Patil, "Design and Study Voltage Characteristics

of Buck Converter by Matlab Simulink," *Proc. 2nd Int. Conf. Trends Electron. Informatics, ICOEI 2018*, pp. 680–683, Nov. 2018, doi: 10.1109/ICOEI.2018.8553695.

[42] P. Gayathiridevi, S. Vijayalakshmi, and K. R. Vairamani, "Discrete controller for high frequency buck converter," *Proc. IEEE Int. Conf. Circuit, Power Comput. Technol. ICCPCT 2013*, pp. 605–610, 2013, doi: 10.1109/ICCPCT.2013.6528978.

Contribution of Individual Authors to the Creation of a Scientific Article (Ghostwriting Policy)

The authors equally contributed to the present research, at all stages from the formulation of the problem to the final findings and solution.

Sources of Funding for Research Presented in a Scientific Article or Scientific Article Itself

No funding was received for conducting this study.

Conflict of Interest

The authors have no conflicts of interest to declare that are relevant to the content of this article.